UCRL-52000-76-1

JAN. 1976

Energy and Technology Review

MASTER

Prepared for U.S. Energy Research & Development Administration under Contract No. W-7405-Eng-48

HOLOGRAPHIC STUDIES OF LASER DISKS

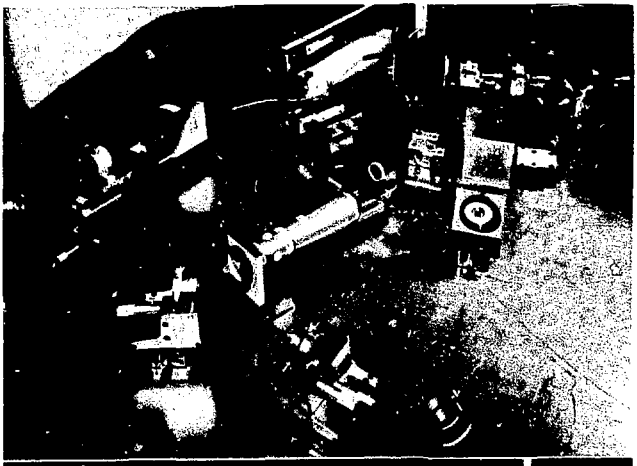

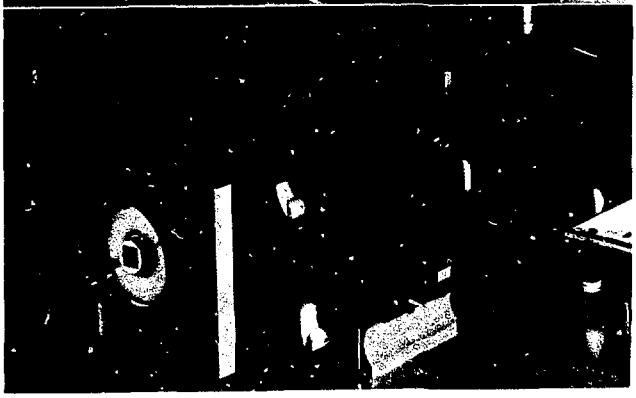

LAWRENCE
LIVERMORE
LABORATORY

Printed in the United States of America
Available from
National Technical Information Service
U.S. Department of Commerce
5285 Port Royal Road
Springfield, Virginia 22151
Price: Printed Copy $____*; Microfiche $2.25

*Pages	NTIS Selling Price
1-50	$4.00
51-150	$5.45
151-325	$7.60
326-500	$10.60
501-1000	$13.60

Distribution Category UC-2

UCRL-52000-76-1
JANUARY 1976

Energy and Technology Review

ABOUT THE COVER

Experimental setup for the Laboratory's new double-exposure holographic interferometry technique (top photograph) and one of the two unique components the reference-beam generator behind this technique (bottom). The second component, an optical phase shifter, is shown in place in the test apparatus (upper left, between the laser source and corner reflecting mirror). Using this test apparatus and associated computer system, we can now measure the wavefront distortion of an optical element with an accuracy of 1/100 of a wavelength; by comparison, resolution with conventional interferometry is limited to 1/20 of a wavelength. For a description of this new technique as it relates to the LLL Laser Program, see the article beginning on p. 1.

Scientific Editor: Ronald B. Carr
General Editors: Charles S. McCaleb
Judyth K. Prono

LAWRENCE LIVERMORE LABORATORY
University of California
Livermore, California/94550

Briefs

The short items on this page announce recent developments of importance. Some of these items may be amplified in future issues; none of this material is reported elsewhere in this issue.

MULTIPHOTON URANIUM ENRICHMENT STUDIED

We recently completed at LLL a series of experiments of major significance to the laser isotope separation program. Their results open up exciting possibilities for economic multiphoton (three- or four-step) excitation processes. We have identified a series of energy levels in atomic uranium with long lifetimes, allowing efficient laser isotope separation with available laser technology. We have also operated a process on the actual wavelengths (using the energy levels identified) that would be used for a full-scale process.

Many photophysical methods for the enrichment of uranium vapor have been proposed, but only two-step photoionization has been reported in the literature. More effective methods involve using multistep (three- or four-step) excitation so that more efficient lasers may be utilized. We have recently undertaken a series of measurements to determine the effectiveness of these schemes.

Previous spectroscopic measurements provided quantitative data only for the first-step transition. The existence of transitions between excited states was known, but there were no measured data on cross sections for these transitions. Also, relevant lifetimes had been measured, but data on excited-state transition probabilities and hyperfine widths were completely lacking. Our experimental measurements of transition wavelengths, transition probabilities, lifetimes, and hyperfine structure have greatly extended the state of knowledge. To date we have measured 50 or 60 lifetimes throughout the uranium spectrum and catalogued hundreds of new levels (although precise quantum numbers have been assigned to only a small fraction). We have also measured about two dozen transition probabilities. These data clearly illustrate the feasibility of multiphoton schemes.

To demonstrate multiphoton uranium enrichment on a laboratory scale, we used three visible dye lasers and an infrared ionization laser (IR kicker) in combination to irradiate a 50/50 uranium-235/uranium-238 vapor. We also characterized additional promising photophysical schemes that are currently being investigated in more detail in the laboratory. In these multiphoton experiments, the cumulative isotope selectivity appears to increase with the number of laser steps. This may have special advantage for the laser isotope separation of weapons-grade uranium and plutonium, where high enrichment is needed.

NEW RADIATION UNITS

Two new radiation units have been approved for use in the International System of Units (SI). The *becquerel* (Bq), named for French physicist *Antoine Henri Becquerel*, who discovered radioactivity in 1896, is the SI unit of radioactivity: 1 Bq = 1 event/s. This unit replaces the curie (1 Ci = 37 GBq). The other new unit, the *gray* (*Gy*), is the SI unit of absorbed radiation, replacing the rad (1 rad = 0.01 Gy) and the joule per kilogram when used to express absorbed radiation (1 Gy = 1 J/kg). The gray is named in honor of British radiobiologist Louis Harold Gray, whose studies laid the foundation for the use of ionization chambers in measuring absorbed dose.

LASERS AND LASER APPLICATIONS

HIGH-RESOLUTION HOLOGRAPHIC INTERFEROMETRY: A NEW TECHNIQUE

The Laboratory has developed a new, more precise technique for measuring the wavefront distortion of plano-optical elements, such as laser disks. With this technique – a variation of double-exposure holographic interferometry – we can measure the distortion of an element with an accuracy of λ/100 (one-hundredth of a wavelength), compared with about λ/20 for conventional interferometry. This high-resolution capability will aid in the evaluation of individual elements as well as in the assembly of large laser systems to minimize total wavefront distortion.

Glass laser systems typically have up to 100 separate optical elements (laser disks, polarizers, lenses, etc.), each of which introduces a small distortion in the laser beam. Cumulatively, these small distortions may produce a significant spatial modulation of beam intensity at the target in laser-fusion experiments. This problem can be controlled by suitably finishing and measuring the quality of all laser components or by compensating for the phase distortion with a correcting optical element.

To understand and control beam aberrations, it is often necessary to measure the wavefront distortion of optical elements with a much higher degree of accuracy than is afforded by conventional interferometry. Adjacent fringes in a conventional interferogram correspond to a phase difference between the interfering beams of 2π, or an equivalent optical-path difference of one wavelength. By interpolating between fringes, we can increase resolution to about 1/20 of a wavelength. If we select optical elements for a laser system on this basis, 100 elements could produce an overall distortion of about three wavelengths. Calculations have shown that a wavefront distortion of only one-half wavelength can result in intensity modulations of up to 75% at the focus of a lens. At the surface of a laser-fusion target – in the intermediate field – the modulations are less intense but still objectionable.

Contact Gary E. Sommargren (Ext. 8573) for further information on this article.

OPTICAL SYSTEM REQUIREMENTS FOR FUSION LASERS

The L.L.L. Laser Program has been conducting an intensive research effort to develop high-peak-power, neodymium glass laser systems for target irradiation. These systems are designed to provide the energy, power, and wavefront uniformity required to spherically implode nuclear fuel targets and achieve thermonuclear fusion through inertial confinement. Several such systems are in operation or under construction.

The requirements on the optical performance of fusion lasers are staggering. Targets as small as 100 μm in diameter must be uniformly irradiated with multiple beams each delivering between 100 and 1000 J of energy. This energy must be delivered in a single, time-tailored pulse whose peak power exceeds 1 TW. To achieve the requisite uniformity and brightness of illumination at this power level, we must thoroughly understand numerous linear and nonlinear propagation phenomena.

To obtain a high-quality beam from the output of a high-power laser system, one must solve all of the usual problems of large optical systems. However, the most difficult problem relating to beam quality is not usually faced in designing optical systems. That is, the index of refraction of all optical elements through which the laser beam passes depends on the beam's intensity. The effect of this interaction between laser radiation and laser disks is that any small intensity irregularity in the beam induces a lens for itself. The induced lens causes the irregularity to be focused and become more pronounced, which in turn induces a stronger lens; so the irregularity grows in dramatic fashion. This self-focusing instability limits the peak power from present Nd:glass laser systems.

At lower power levels, where the aberrations due to self-focusing are not apparent, passive aberrations in the laser optical elements limit the focusing properties of the laser beam and cause nonuniform intensity distributions at the laser focus. We have made dramatic progress in not only measuring but also controlling linear and nonlinear beam distortion in Nd:glass lasers. The accompanying article discusses a recent development in our ability to measure small aberrations in optical components.

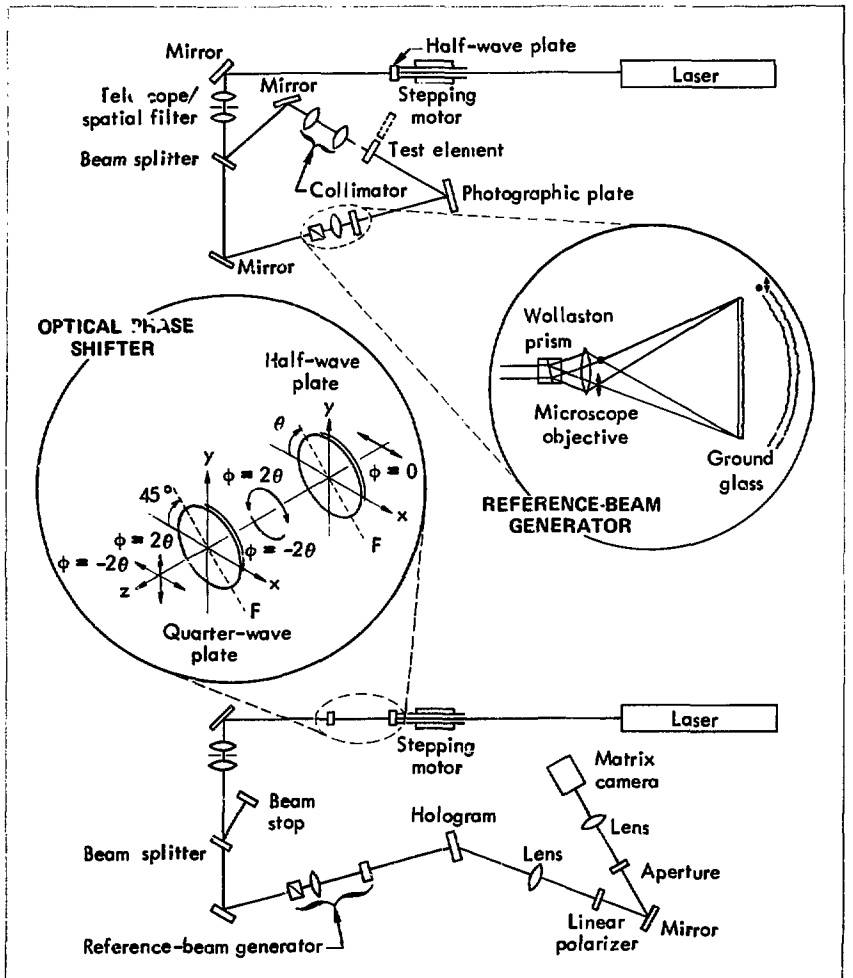

Fig. 1. Experimental setup for recording (top) and reconstructing (bottom) the double-exposure hologram. The two unique components distinguishing this setup from conventional holographic interferometry are shown in the two insets: a polarization-dependent, common-path reference-beam generator (right) and an optical phase shifter (left). In the reference-beam generator, the input beam's vertical (dot) and horizontal (arrow) components are transmitted by a Wollaston prism and microscope objective onto a ground-glass screen, which generates the two uncorrelated, orthogonally polarized speckle patterns used to record and reconstruct the hologram. The optical phase shifter allows precise control of the relative phase ($\Delta\phi$) between the two reference beams used in reconstruction. The laser input beam to the optical phase shifter is linearly polarized in the horizontal direction; the output is two beams orthogonally polarized in the horizontal and vertical directions with a phase difference of 4θ.

To measure wavefront distortion with higher phase resolution, we first need a method that is independent of the quality of the auxiliary optical elements. Double-exposure holographic interferometry is one such method. It provides a measure of the difference between two states of the optical test system, thereby eliminating the effect of the auxiliary optical elements present for both exposures. It does not provide adequate resolution, however. As with conventional interferometry, adjacent fringes in the resulting interferogram correspond to an optical-path difference of one wavelength. Although different schemes have been devised to interpolate between fringes and increase resolution, they are all necessarily based on comparing intensities between different spatial positions in the interferogram. Because intensity depends not only on phase variations but also on the intensity profiles of the interfering beams and on the detector's nonlinearity, these schemes are limited to a modest gain in resolution.

If we could continually vary the relative phase of the interfering beams, however, the intensity at different times (but at the same spatial position) could be compared. For a relative phase change of 2π, the intensity at every position in the interferogram would vary sinusoidally through one period. The phase of these variations would then be precisely equivalent to the wavefront distortion of the optical element under test.

We have developed a variation of double-exposure holographic interferometry that allows us to produce these sinusoidal variations and thus to measure plano-optical elements with an accuracy of $\lambda/100$. The resulting measurement is in the form of a computer-generated phase array. From these arrays, both contour and three-dimensional perspective plots of wavefront distortion can be displayed. The computer can also use these arrays to choose individual elements and their orientation so as to minimize wavefront distortion for a particular laser system.

New Interferometry Technique

Starting with the experimental setup and procedure of conventional double-exposure holographic interferometry, we have added two unique components: a polarization-dependent, common-path reference-beam generator and an optical phase shifter. It is the combination of these components that permits high phase resolution.

Our basic experimental setup for recording the two holograms is shown in the top diagram of Fig. 1. The source here is a helium:neon laser with a linearly polarized output beam. This beam passes through a half-wave plate mounted in the hollow shaft of a precision stepping motor. By rotating the half-wave plate, we can introduce any orientation of linear polarization into the optical system. The polarized beam is then split at a beam splitter; the object beam passes through a collimator and on to the photographic plate, the reference beam passes through the reference-beam generator. This latter component, shown in the right inset of Fig. 1, generates either one of two reference beams or both simultaneously, depending on whether the polarization of the input beam is horizontal, vertical, or a linear combination of both.

The input beam generally contains both horizontally and vertically polarized components. In the reference-beam generator, they are transmitted with a slight angular divergence by the Wollaston prism and focused with a microscope objective to produce two point sources with a small separation (approximately 60 μm). These sources illuminate a ground-glass screen, which then generates two orthogonally polarized speckle patterns at the photographic plate. The speckle patterns are uncorrelated because of the small but finite separation of the point sources. When the input beam contains only horizontal or only vertical components, just one of the reference beams is generated.

To record the first (initial-state) hologram, we set the half-wave plate so that the laser beam is horizontally polarized and then make an exposure of the test element. Next, the test element is removed from the beam (shown dotted in Fig. 1), while the half-wave plate is rotated 45° to give a vertically polarized beam. The second (final-state) hologram is then exposed, and the photographic plate is removed, processed, and replaced in its original position.

Our experimental setup for reconstructing the holograms is shown in the bottom diagram of Fig. 1. Note that here a quarter-wave plate is placed after the half-wave plate. These two elements comprise our second unique component, the optical phase shifter, shown schematically in the left inset. When a horizontally polarized beam passes through the half-wave plate, which is oriented with its fast axis (F) at the angle θ, a linearly polarized beam with an orientation of 2θ is produced. This beam, however, may also be thought of as the combination of two beams of opposite circular polarization with a relative phase difference ($\Delta\phi$) of 4θ. When the beam next

passes through the quarter-wave plate, these orthogonal circular polarizations are converted to horizontal and vertical polarizations that preserve the 4θ phase difference.[1] The relative phase between the two beams can therefore be precisely controlled by the stepping motor, in incremental steps of $2\pi/500$.

To reconstruct the holograms, we only use the system's reference-beam arm. From the optical phase shifter, the two polarized beams pass through the reference-beam generator to produce both reference beams simultaneously, which then illuminate the holograms. The two reference beams and two holograms give a total of four reconstructions. Each reference beam and its uncorrelated hologram produce a noise background. Each reference beam and its correlated hologram produce a reconstructed wavefront. Because these wavefronts are orthogonally polarized, no interference occurs. It is therefore necessary to image them through a linear polarizer oriented at 45° to produce an interferogram.

A photograph of our optical test apparatus is shown in Fig. 2. The resulting double-exposure hologram gives the interference between the wavefront that passes through the optical element under test and the wavefront that passes through the air occupied by the element. The advantage of this technique over conventional double-exposure holography is that the relative phase between the reconstructed wavefronts can be precisely controlled by varying θ. Then interfacing to a computer and using synchronous detection, we can determine the wavefront distortion of an optical element with great accuracy.

Holographic Data Analysis

The coupling of the optical test apparatus to the computer system is shown schematically in Fig. 3. The interferogram is detected by a self-scanned photodiode matrix camera free running at about 50 ms per frame. Video signals (i.e., photodiode levels) and their associated clock pulses, along with the end-of-line and end-of-frame synchronization pulses, are sent to the controller. The controller, which was specifically designed for this system, then sends the video information and synchronization signals to the computer and sends appropriate pulses to the stepping motor.

From the video signal, coincident and quadrature components of the intensity at each photodiode position are calculated as θ varies through a total of $\pi/2$. The phase at each position is then calculated from these components and stored in an array. This phase array is searched for 2π discontinuities and corrected until the phase is continuous over the entire array. Finally, the phase at the center position is subtracted from all positions, making the center position a reference point with phase zero.

The maximum values of the phase array are displayed on the terminal screen, after which the operator keys in an appropriate contour interval. A phase contour map of the test element's wavefront

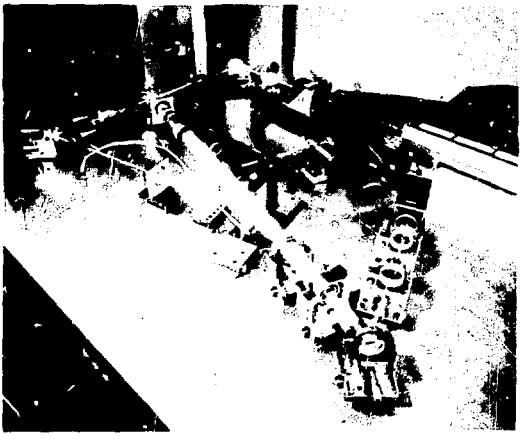

Fig. 2. *Optical test apparatus (shown in reconstruction configuration) for measuring wavefront distortion.* The "pencil" beam of laser light is shown going through the reference-beam arm of the optical system, finally dispersing through the ground-glass screen (white square) and onto the hologram in the black plate holder. The diffuse beam represents the path the object beam would follow – from the collimator, through the test element (displaced aside here), and onto the photographic plate – in the recording step. When a hologram is reconstructed, however, this beam is stopped after the beam splitter; it is shown here simply for illustration. To the right of the hologram, the reference beam passes through a lens and linear polarizer, reflects off a mirror, and then passes through an aperture and another lens to the matrix camera (black box).

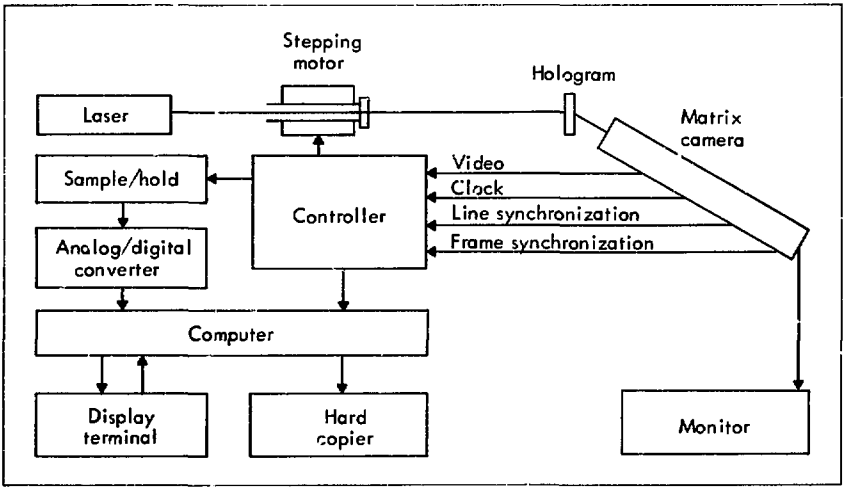

Fig. 3. System diagram for the modified holographic interferometry technique developed at LLL. The optical test apparatus is represented at the top here in condensed form.

distortion is then displayed on the screen. To aid the operator in distinguishing maxima from minima, a three-dimensional perspective plot is also displayed. Printed copies of these plots, as shown in Fig. 4, can be made at this time and the phase array may be put in long-term storage for future use.

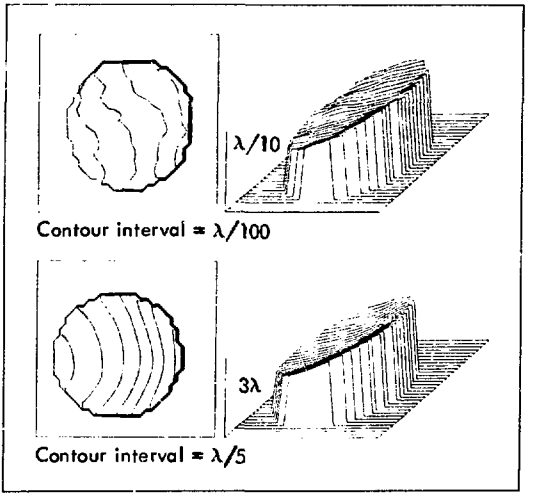

Fig. 4. Measurements of wavefronts transmitted by good- (top) and poor-quality (bottom) glass disks. For the ideal glass disk, the top of its perspective plot would be perfectly smooth and horizontally level.

To measure the errors inherent to our system, we made a double-exposure hologram without the presence of a test element. In theory, the phase array from such a hologram should be zero at each position; because of air turbulence between exposures, we found that accuracy was limited to about $\lambda/100$ over the entire array. This is much higher resolution, however, than is possible with conventional holographic interferometry.

We have used our modified technique to measure the wavefront distortion of a number of glass disks. Sample results for a good- and a poor-quality disk are shown in Fig. 4. On the basis of such plots, we can first establish more stringent criteria for selecting optical elements, and second, compensate for those distortions still introduced into the laser system. From the phase arrays stored in its memory, the computer can determine the optimal assembly of these elements to minimize total distortion of the entire laser system.

To date, the disks tested have been only 50 mm in diameter, but larger elements can be similarly measured simply by changing the collimator and adding a collecting lens after the test element. Our test apparatus can thus be adapted to measure the wavefront distortion of the optical elements needed for any laser system.

Further Applications

Although our new interferometry technique is described here in terms of evaluating optical elements, it is not restricted to this application. In a more general configuration, the test apparatus can also be used to measure extremely small differences between two states of any object (solid, liquid, or gas) altered between exposures. The test object may be either specular or diffuse, reflecting or transmitting.

For example, we have used our test apparatus to measure the surface deformation of a steel bar due to cooling. From such measurements, the coefficient of thermal expansion can be calculated with great accuracy. In general, by applying this technique to those areas of nondestructive testing where conventional holographic interferometry is presently used, we can increase measurement accuracy by a factor of 10 to 100.

Key Words: holography; interferometry; interferometry instrumentation, laser - applications, laser interferometry, optical testing; wavefront reconstruction.

INITIAL BASEBALL-II PELLET EXPERIMENTS SUCCESSFUL

To generate a startup plasma for the Baseball-II CTR experiment, we plan to irradiate solid ammonia pellets with a laser beam. In-flight pellet irradiation has recently been achieved. The next step is to incorporate this laser-pellet system in the Baseball facility for plasma-buildup experiments.

In December, the first in-flight irradiation of frozen ammonia pellets with a pulsed CO_2 laser beam was achieved by the Baseball-II group. This result represents an important step in the development of a technology for creating startup plasmas in magnetic mirror fusion experiments. The function of the startup plasma is to provide a target capable of initially ionizing the beams of energetic neutral atoms that are injected; this warm target plasma thus seeds the trapping process. Continued neutral-beam injection then sustains the desired high-temperature plasma for confinement studies.

In the 2XIIB experiment (described in last November's *Energy and Technology Review*, p. 1), startup is achieved by injecting the target plasma into a time-rising magnetic field from plasma guns located outside the confining magnet. In Baseball II, however, and ultimately in mirror reactors as we presently envisage them, the magnetic field is steady in time, provided by a superconducting magnet. Thus pulsed-field trapping techniques cannot be used to form the target plasma. Given this static field, one attractive startup alternative calls for generating the warm target plasma by heating a solid pellet with a pulsed laser beam. In contrast to laser fusion, this technique does not involve subnanosecond pellet compression and heating but rather aims for a more leisurely ionization over a period of tens of nanoseconds. Target-plasma ions need only be warm enough (1 keV) to ensure their confinement within the magnetic mirror for about 2 millisecond sufficient time for ionizing enough neutral-beam atoms to fill the plasma volume.

The pellet startup approach chosen for Baseball II is to project frozen ammonia pellets in free flight to the laser focal spot at the center of the confining magnetic field. Because no supports are needed for the pellets and surfaces cooled with liquid nitrogen freeze out excess ammonia, this approach satisfies an important requirement for plasma confinement schemes namely, that the target plasma be generated in high vacuum. Initial laser-irradiation experiments have been successful.

To date, our tests have been conducted on an apparatus external to the Baseball magnet, using a small 25-J CO_2 laser. Pellets are generated at the rate of 15 000/s from a liquid stream of ammonia located 3.2 m from the laser focus (Fig. 5, top). A selected fraction (~20%) is electrically charged and directed through a 2.3-mm orifice into high vacuum. Several centimetres beyond the orifice, the pellets freeze. Pellet dispersion at this point is so great that few would intercept the downstream laser focus. Because the pellets are charged, however, they can be steered electrically. The pellet's position at two points in flight is sensed electrically to an accuracy of ±15 μm

Contact Charles C. Damm (Ext. 7153) for further information on this article.

BASEBALL-II EXPERIMENT

Baseball II – a major CTR companion experiment to 2XIIB – uses a superconducting magnet to confine a plasma. Confinement times of seconds have been achieved although only at relatively low densities (~10^9 cm^{-3}) and low ion energies (1 to 2 keV). The immediate goal is to reach a high-density regime, ~10^{13} cm^{-3}, with ion energies above 10 keV; in the process, shorter confinement times, approaching 5 milliseconds, are expected. The critical factor is to form a target plasma within the steady-state confining magnetic field that can be subsequently heated by neutral beams to build up a hot, high-density plasma.

One highly promising startup approach is to generate a warm target plasma by the laser-irradiation of a small, solid pellet. Work is now under way to incorporate pellet startup in the Baseball experiment. Development of such a technique is important because future CTR experiments – such as MX and FERF – and mirror reactors as now envisioned will all use superconducting magnets.

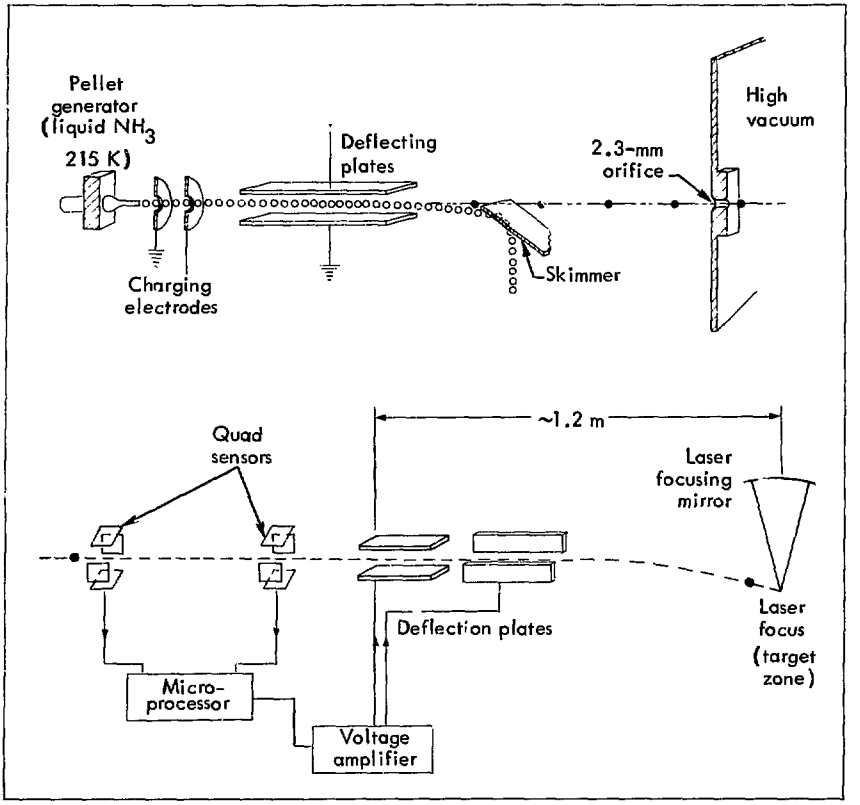

Fig. 5. Ammonia pellet charging and deflection scheme (top) with pellet guidance and delivery system (bottom) for Baseball-II experiment. Total length of apparatus from pellet generator to laser focus is 3.2 m.

(Fig. 5, bottom). A small microprocessor then computes the trajectory correction required to direct the pellet to the focus and applies the necessary deflection voltages to a set of parallel plates. (At this point, we are working with about one pellet per second.) This sensing and computation is accomplished during a flight time of about 30 ms. Beyond the deflecting plates, the pellet is again in free flight for the final 80 cm to the focus, simulating penetration to the center of the Baseball magnet.

Our present pellet guidance system reduces tenfold the pellet dispersion radius at the focal plane, with the pellets arriving within ±1 mm of the center. This concentration puts about one pellet per minute through the focus, more than adequate for preliminary experiments on Baseball II. A pair of visible laser beams signal the pellet's arrival by reflected light and trigger the pulsed CO_2 laser to ionize and heat the pellet. Energetic ions in the 100-eV range have been detected on charge collectors located around the pellet, indicating an expected level of heating.

Our next step is to introduce the pellet stream into Baseball II, where a more powerful 300-J CO_2 laser is located. With this higher intensity irradiation, we

expect ion energies to reach the desired 1-keV range. At the same time, the pellet guidance system will be improved to account for the small variations in pellet charge-to-mass ratios presently observed and assumed responsible for the residual dispersion. Our goal is to place every processed pellet within ±0.05 mm of the magnet's center, so that each will pass through the 0.2- to 0.4-mm-diam laser focal spot. With this accuracy, the energetic neutral beams can be properly timed, and plasma-buildup experiments in Baseball II can proceed. We anticipate beginning these experiments within the next several months.

Key Words: Baseball; CTR project; fusion; magnetic mirrors; mirror machines; plasmas – heating.

SUBSURFACE GEOLOGIC MAPPING BY ELECTRICAL SIGNALS

For coal field characterization and other geophysical applications, LLL has developed and extensively tested electrical methods for probing subsurface geologic structures. The basic principle is to "map" the region of interest by electrical signals transmitted between probes (transmitter/receiver pairs) at specified depths on opposite sides of the region, producing a network of signals that vary according to the electrical properties of the media through which they have passed. From this map and previous experimental data, we can mathematically reconstruct the structure of the region of interest, including anomalies, lenses, water-bearing strata, and the like.

Using these methods, we have conducted field studies on the effects and extent of high-explosive fracturing of coal and on fluid-flow characteristics through coal beds. We have successfully used electrical methods for preliminary subsurface surveys to find such anomalies as forgotten mine tunnels.

Our research into the electrical mapping of subsurface geology dates back to the late 1960's. It had long been known that electrical waves lose different amounts of energy in passing through different materials, the extent of loss depending on the electrical resistance of the media through which they pass. Yet this characteristic had not been exploited for studying underground structures. The usual techniques involved monitoring gravitational anomalies and performing acoustic soundings. We believed that electrical mapping, if feasible, would prove superior in both accuracy and completeness. The potential applications were many: mining and tunneling; reactor site studies; identification of ore bodies, oil pools, salt domes, etc. Accordingly, we set out to solve the practical problems of electrical mapping, such as data collection and interpretation, development of a reference base (specific electrical characteristics of different media), and techniques for compensating for (or discounting) reflection and refraction of the electrical waves.

Our first field experiments were performed in a private mine in Arizona, at the NORAD complex inside Cheyenne Mountain in Colorado, and in the Wawona Tunnel at Yosemite National Park. The purpose was to determine the electrical properties of hard rock at high frequencies by propagating 2- to 50-MHz electromagnetic waves through up to 300 m of rock (achieved at Yosemite). Experimental and data-analysis techniques were then developed for experiments in 1972 in Alaska's Brooks Range, near Lizbourne, to determine the electrical properties of permafrost rock.

In 1974 these techniques were refined and new ones developed for a series of experiments at Kemmerer, Wyoming, where the pre- and post-shot properties of a coal seam were evaluated for LLL's coal gasification program (see Fig. 6). More recently, we completed a study of the fluid-flow characteristics of the coal seams at Hoe Creek, Wyoming, a site of possible future coal gasification experiments. Also, the Department of Transportation has now funded some theoretical studies on techniques – improved methods of data collection and interpretation – to reduce cost overruns on urban tunneling projects (i.e., for rapid transit).

At present, new experimental techniques are being developed, along with more sophisticated analytical tools for reducing data. A scale-model test facility has been built for performing experiments under carefully

Fig. 6. Setting out dipoles for four-probe, very-low-frequency test measurements at Kemmerer, Wyoming, in support of the LLL coal gasification program. This and other techniques allow us to develop accurate three-dimensional "maps" of subsurface strata.

Contact R. Jeff Lytle (Ext. 8214) for further information on this article.

controlled conditions to evaluate the accuracy and sensitivity of measurement and data-reduction techniques. We have now developed three major electrical-mapping methods: a high-frequency (3- to 30-MHz) attenuation technique, a very-low-frequency (20-Hz) four-probe technique, and a general technique called wave tilt.

High-Frequency (Attenuation) Method

Recent improvements in our high-frequency technique have included refinement of our analytical codes for reducing field data (described below) and two novel developments:

- Short active antennas for the receiving probes. These are wideband (0.5- to 25-MHz) antennas about 50 cm long with the active elements incorporated into the antenna. They are about 5 cm in diameter and 60 cm in overall length (much shorter than previous antennas) and can be operated in water.
- A computer program to correct for near-field effects. Quite often, because of the spacing between existing drill holes or test bores in which we emplace the probes, the transmitters and receivers are located such that the receiver is in the near field of the transmitter. Errors could result if corrections were not made. Our program is written for a pocket calculator so that data can be corrected in the field.

The general principle of the attenuation method is shown in Fig. 7. A transmitter and receiver are emplaced in drill holes on opposite sides of the region of interest (the zone to be mapped), and a high-frequency wave is generated from the transmitter. The depths of both probes and the horizontal distance from transmitter to receiver are known, hence we know the length of the transmission path (i) and its angle (θ) relative to the horizontal. The attenuation of the high-frequency wave along this path is a function of the electrical properties (relative permittivity and skin depth) of the media through which it passes.

As the first step in interpreting the attenuated signal, we impose a model – a set of zones delineated by arbitrarily spaced vertical and horizontal lines – on the region of interest. It is not necessary for the drill holes to be plumb. The transmission path traverses a straight line from transmitter to receiver, traveling a distance D_{ij} through the arbitrary zone j. Note that the model assumes that the signal follows only one path from transmitter to receiver, ignoring other modes of propagation: i.e., reflection from the surface or travel up one drill hole, along the surface, and down the other hole. In the operating situation, it is possible to detect these modes and choose operating frequencies and depths to minimize their effects. Also, the assumption is made that there is no reflection and refraction when passing from zone to zone. This is true if the changes in electrical parameters from zone to zone are gradual. All these assumptions tend to introduce somewhat uniformly distributed noise in the data.

Mapping and accurate decoding of the individual signals require a sizeable number of transmissions to define the region of interest. By varying the depths of transmitter and receiver, we get a set of pathways such as shown in Fig. 8. In this case, the data have been taken in 3-m increments from 6 to 27 m below the top of a coal seam, with a 9-m horizontal spacing between drill holes. The signal behavior varies as the positions of transmitter and receiver are changed.

The computer algorithms used to reconstruct the region of interest come mostly from those developed

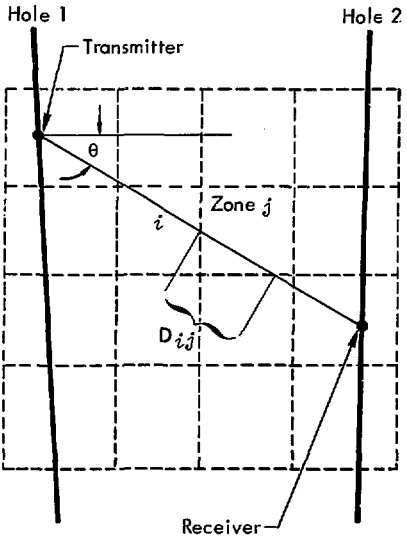

Fig. 7. The region to be analyzed is modeled as rectangular zones specified by arbitrarily spaced vertical and horizontal lines. From transmitter to receiver is a representative straight-line path i. D_{ij} is the distance traveled through zone j by the path i.

by medical researchers to portray the interior of a human brain or other body parts from a series of x-ray projections. This study, called tomography, is analogous to subsurface geologic mapping. The approach is to approximate the electromagnetic equations that describe the signal behavior from a given transmitter location to a given receiver location as a linear system of equations relating the signal attenuation and distance D_{ij} with the unknown electrical properties (relative permittivity and skin depth) of the arbitrary zone j. We then solve for relative permittivity and skin depth as functions of the magnitude and phase of the received signal, taking into account cable losses, the transmitted power, and the gain of the antennas. Details of these mathematic operations have been published, together with descriptions of the algorithms used.[2]

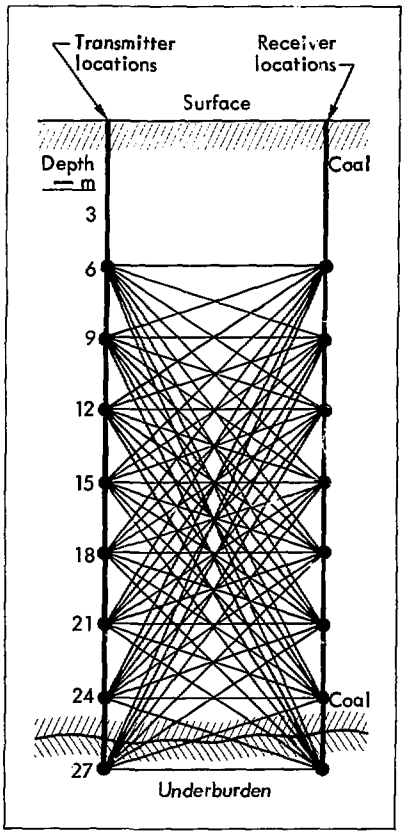

Fig. 8. Transmitter and receiver sites (in metres beneath the overburden) for high-frequency determination of the medium's uniformity. Most sites are within the coal seam; two are below the coal, in the underburden. Shown here are all possible straight-line paths for the transmitter/receiver pairs.

One of these algorithms is the algebraic reconstruction technique (ART), which computes the electrical parameters for each cell of the model. If the region of interest is homogeneous, the cells yield similar values. If not, the anomaly stands out. Figures 9 and 10 show ART reconstructions of actual data from Kemmerer taken before high-explosive fracturing of a coal seam. Note that the values are quite similar from cell to cell throughout the seam, but the interface between the seam and the underlying clay is clearly defined in the skin-depth measurements (Fig. 10). The dielectric constant (Fig. 9) apparently is not as good a diagnostic.

High-frequency techniques are also used to characterize the movement of fluids (e.g., salt water or high-resistivity water) through geologic media. Coal gasification by the proposed LLL technique requires adequate permeability in the coal seam to maintain a process reaction induced by injecting oxygen from the surface; our studies with fluids provide advance information on this important characteristic. Relative to normal ground water, salt water attenuates the signal between the transmitter and receiver; high-resistivity water enhances the signal. The technique in either case is to inject the fluid and watch for its spread through the coal seam, producing a time plot of the permeability. By scanning the seam from different vantage points, we can build up an accurate three-dimensional profile showing high-permeability zones, anomalies (e.g., big fractures), discontinuities, and asymmetrical flows (those moving in a preferential direction).[3]

Figure 11, a signal-strength plot from Kemmerer, illustrates the basic technique. Between transmitter and receiver, we inject the test fluid (salt water in this case) and measure the signal change. The time scale here is short: 3 h. The attenuation curve is steep and almost straight-line, suggesting rapid, uniform spread of the salt water and, thus, uniform high permeability. This was a preliminary study. The data would have to be confirmed later by detailed studies.

At Hoe Creek we performed experiments of greater complexity. Involved in these were eight mapping sites

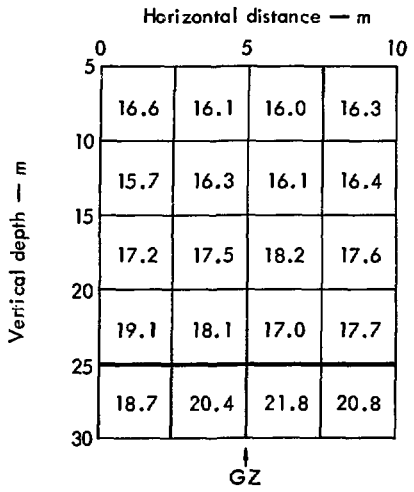

Fig. 9. ART reconstruction of data from Kemmerer, Wyoming, showing the relative permittivities (dielectric constants) of a coal seam and underlying clay deposit.

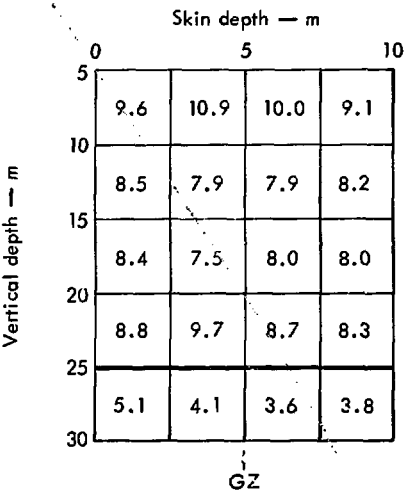

Fig. 10. ART reconstruction of Kemmerer data showing the *skin-depth values for the coal seam* and clay underburden. Note that the coal-clay interface is clearly defined.

(see Fig. 12) and a multilayer deposit consisting of 30 m of overburden, a 5-m upper coal seam, 3 m of clay, an 8-m lower coal seam, and clay underburden. The fluid for these experiments was high-resistivity water. There were several problems, including the likelihood that test fluid injected into the upper coal seam would percolate into the sandy clay overburden.

Experiment #1, in the lower seam, tested injection into well #8 with the transmitter in this well and the receivers in wells #9, 11, and 13, respectively. The results are revealing. Arrival of the test fluid – indicated by a sharp rise (enhancement) of the signal – was delayed about 24 h for wells #9 and 11; well #13 received almost no test fluid. Our interpretation is very little communication in the lower seam between well #8 and the other locations, plus the probability of asymmetric flow. The delay also probably reflects the time needed for the test fluid to move the natural ground water in this seam.

In experiment #2 (upper seam), we experienced what we interpret as percolation into the overburden. The fluid was injected into well #12, which also housed the transmitter. The receivers were in wells #3, 9, and 11. The results show very rapid dissemination

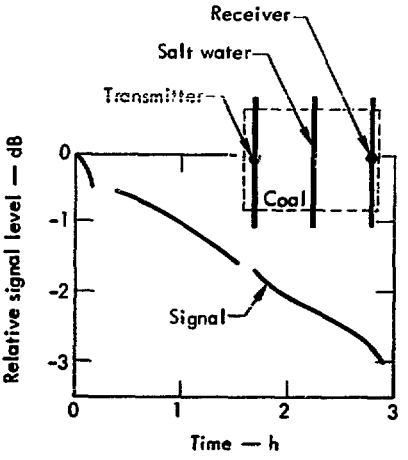

Fig. 11. Steepness and uniformity of this attenuation curve, obtained at Kemmerer, suggest rapid, uniform spread of salt water through a coal seam and, hence, uniform high permeability to fluid flow. From this we infer high permeability to gases, which is a requisite for the LLL coal gasification process.

of the fluid (high permeability) followed by an attenuation probably caused by the percolation.

In experiment #3, we returned to the lower seam. The transmitter here was in well #8 and the receivers in wells #11 and 13. The test fluid was injected into well #4, which is steel-cased down through the overburden but open to the coal seams. As shown in Fig. 12, well #4 is slightly off-center with respect to transmissions from well #8 to the receivers; the resulting effect appears in the enhancement curve (lower right) as a 2-h delay before a sharper enhancement that signals arrival of the test fluid in the straight-line path from transmitter to receivers. We interpret the results from this experiment to mean moderate permeability.

These experiments, like those at Kemmerer, are considered preliminary. They have given us a chance to check out our equipment and techniques before undertaking a full-fledged diagnostic effort such as required for an actual coal-gasification experiment. The new short active antenna is one result of this field testing (a predecessor was tested at Hoe Creek). At Hoe Creek, also, we were able to check out the *near-field-correcting computer program* under field conditions. Details of this program are now being readied for publication.[4]

Very-Low-Frequency Four-Probe Method

Our very-low-frequency (20-Hz) resistivity method was used at Kemmerer to characterize the general experimental area and to look for anomalies such as tunnels. In these experiments, we used a four-probe configuration (Fig. 13) in which two pairs of metal probes (dipoles) are driven into the ground a distance *a* apart, depending on the depth to be probed. A current source is connected to one of the pairs (the

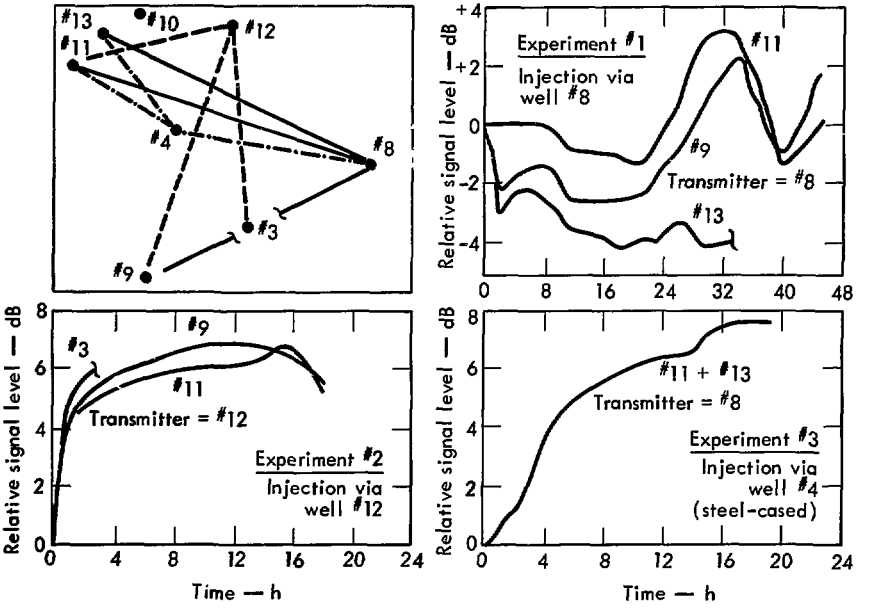

Fig. 12. Data from three permeability experiments at Hoe Creek, Wyoming, in wells arranged as shown at the upper left. Two coal seams are involved, and the test fluid is high-resistivity water, which produces a signal enhancement rather than attenuation. Experiment #1 (upper right) suggests minimum communication between well #8 and the other wells in the lower coal seam. Experiment #2 (lower left) shows high permeability in the upper seam. Experiment #3 (lower right) shows moderate permeability in the lower seam around well #4.

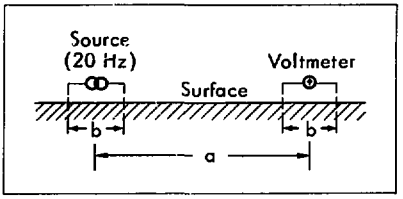

Fig. 13. This configuration for four-probe resistivity measurements gives the best signal-to-noise ratio and also permits large separations between transmitter and receiver. The depth probed is a function of the separation between the transmitter and receiver pairs (a); resolution and signal strength depend on the spacing between the pins (b). The excitation frequency is 20 Hz to avoid polarization of the electrodes.

transmitter); measurements are then made of the voltage induced across the other pair (the receiver). The apparent resistivity is calculated as the ratio of received voltage to transmitter current.

Both vertical surface profiles (variation with depth) and horizontal subsurface profiles (variation with lateral position) can be determined by this technique. For a vertical profile, the center of the array is fixed over the region of interest and the spacing a is varied; larger spacings "see" deeper than smaller spacings. For a horizontal profile, a constant spacing of a is maintained as the array is moved along the ground. The technique can be applied below the ground by using a pair of drill holes. Data reduction proceeds by a modeling process similar to that for the high-frequency method. Again, details are now being readied for publication.[5]

Figure 14 shows the results of a surface scan at Kemmerer to find a cavern caused by earlier tunnel mining. The variation in resistivity as the four-probe array moves along the surface is typical of a void. Subsequent drilling revealed a rubble- and water-filled cavern.

Figure 15 compares the traces from two four-probe vertical scans with those from two four-probe horizontal scans. Clearly evident are anomalies produced by earlier tunneling. As shown in Fig. 16, the four-probe scan is equally effective in identifying the splitting of a coal seam into two seams separated by a sand lens.

Figure 17 shows the "shot hole" at Kemmerer before and after detonation of the high explosive. A definite anomaly exists after the explosion, with

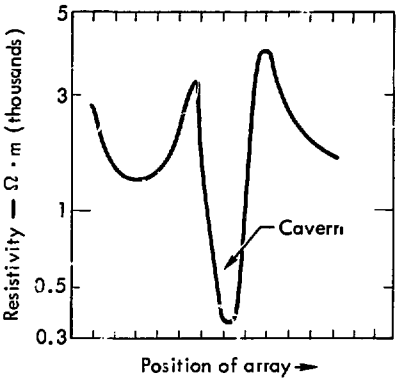

Fig. 14. Four-probe surface measurement at Kemmerer, Wyoming, identifies a cavern created by earlier tunnel mining.

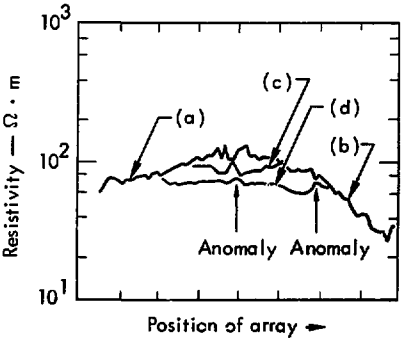

Fig. 15. Four-probe vertical and horizontal profiles at Kemmerer show various anomalies. The (a) and (b) traces are vertical profiles with dipole-to-dipole separations of 123 and 72 m, respectively. The (c) and (d) traces are horizontal profiles with separations of 90 and 60 m. In all cases, the pin-to-pin spacing at the dipoles is 3 m.

boundaries extending out to about 3 m on either side of the shot hole.

This technique could be used to measure the bulk resistivity of a coal outcropping, as a first step in calculating porosity. We would determine the resistivity of the formation water by measuring water samples, and then calculate the porosity as a function of both these resistivities (coal and water). This

procedure could not be verified at Kemmerer because of the absence of coal outcroppings.

Wave Tilt

This method – less well characterized than the others – proceeds from the fact that a wave propagating along the surface of a lossy medium must tilt in the direction of the propagation to satisfy the boundary conditions on the fields. Wave tilt is defined as the ratio of the horizontal and vertical components of the electric field of the propagating wave.

Our 1972 experiments in Alaska were by hole-to-hole transmissions and four-probe methods, but it occurred to us later that wave tilt could be used to determine the thickness of the active layer in the permafrost zone. The active (surface) layer, which thaws in summer and refreezes in winter, varies from 1 to 500 m thick depending on location and time of year. Knowledge of this thickness would be helpful for building any linear structures and especially the Alaska pipeline, because thickness of the active layer dictates the pipe-support methods.

The basic procedure, as we envision it, consists of setting up a transmitter to propagate a surface wave in the region of interest. Then one drives or slowly flies across this region with a receiver and recording apparatus to monitor the wave tilt as a function of position and frequency. As the frequency varies, the reflection from the underlying, permanently frozen layer causes constructive and destructive interference as a function of the thickness of the active layer. Thus its thickness is deduced from the "oscillation" rate of the wave tilt.

The wave-tilt method has a significant advantage over the high-frequency and four-probe methods in that it does not require holes to be drilled or pegs to be driven into the ground. By this method it should be possible to conduct preliminary surveys of extremely large areas to identify places of interest for closer examination by other methods.

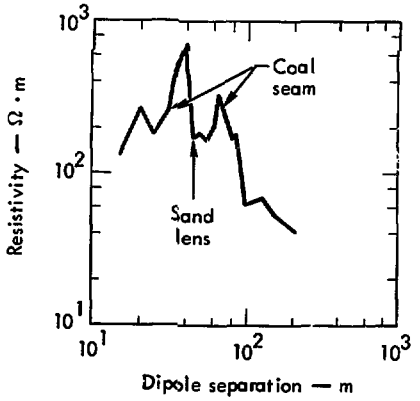

Fig. 16. Four-probe surface measurement at Kemmerer shows the splitting of a coal seam into two seams separated by a sand lens.

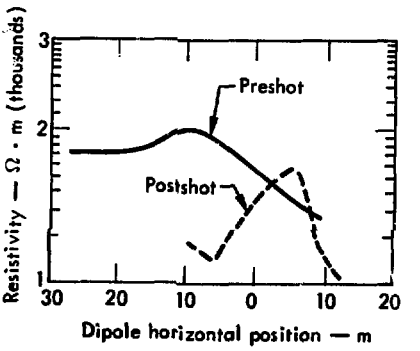

Fig. 17. Pre- and post-shot four-probe measurements at Kemmerer reveal an anomaly caused by a high-explosive detonation in a coal seam. The dipole separation for these measurements was about 45 m; the pin-to-pin spacing of the dipoles was 9.1 m.

Future Directions

Our electrical geophysical probing effort has proceeded from an experimental determination of the electrical properties of hard rock to the development of various techniques, at high and low frequencies, for conducting studies ranging from initial site surveys to detailed mapping. The Kemmerer and Hoe Creek experiments have proved the utility of the techniques for subsurface mapping, fluid-flow mapping, etc. The techniques are being improved and new ones developed by further computer studies and by use of the scale-model facility. We envision further applications to several important areas:

- Identification of ore bodies, oil pools, salt domes, etc.
- Mapping of the burnfront in oil-shale and coal-gasification recovery experiments.

- Reactor site studies to identify any subterranean features that might imperil the reactor.
- Resource mapping at mines to follow the productive deposits, especially those appearing to pinch out but suspected of reappearing elsewhere.
- Predetermination of the underground structures for excavation projects, for purposes of scheduling the equipment types and duration of need for heavy excavating equipment.

The latter is particularly interesting with respect to urban tunneling for underground transit systems. Equipment costs are quite high for such tunneling; expenses mount rapidly when equipment to cut granite stands idle while the tunnelers remove gravel from an unsuspected subterranean stream bed. Electrical mapping is a sensible alternative to the traditional practice of punching test holes at 15-m spacings along the transit route and then inferring the intervening geology.

Key Words: electromagnetic waves – applications; electromagnetic waves – mathematical analysis; fluid flow – computations; fluid flow – measurements; fluid flow – models; geophysics; remote sensing.

A FRAMEWORK FOR STRATEGIC THOUGHT

The Soviet Union, in three decades, has moved from gross inferiority to strategic military parity with the United States. Many within (and outside) U.S. governing circles view this situation with equanimity – as a position of stability from which we can build manifold cultural and economic bridges to the U.S.S.R., lessening the stings of political confrontation and reducing the risks of a mutually unwanted war. But does parity in fact imply stability? What are the long-range implications?

Often disregarded is the question of how the Soviets view parity. In their eyes, does the present U.S. posture of mutual assured destruction appear acceptable? Does it imply less – or greater – risk of war? What are the Soviets' likely long-range responses to parity?

In this article, Robert Squire of this Laboratory explores some principles and implications of military power relationships. The article is based on material presented last year by Dr. Squire to the Military Operations Research Society.

The danger of war remains a spectre on the world scene, made all the more sinister by the existence of weapons of mass destruction and evidence that nations continue to be willing to engage in wars of extraordinary ferocity. Efforts to blunt this violence have centered on talks and treaties placing limits on military forces, particularly those arms lending themselves to widespread destruction of populations and socioeconomic national bases.

This paper attempts to go behind the visible actions of these negotiations and agreements, important as they are, to the concealed and unrealized fundamental assumptions on which they may rest. We are concerned here with the perceived and real dependence of the probability of war on the balance of military force. The perceptions under investigation are those of the United States and the Soviet Union. The reality is the objective of this paper. At issue is the validity of the belief that an essential equivalence of strategic strength – parity – between our two nations minimizes the probability of war.

Strategic force balance – defined here as a range of conditions from overwhelming U.S. military superiority through parity to overwhelming Soviet military superiority – is taken as a prime determinant of the probability of war. Another determinant is the perceived ability of the victim (either nation) to inflict catastrophic retaliatory damage on the aggressor. Of course, factors other than force balance or damage potential – economic, political, and social factors – may effect a desirable reduction in the probability of war. For simplicity's sake, however, we confine our remarks here to the first two fundamental determinants and trace their implications. Because the ensuing probability plots are intended only to convey trends, the parameters on these plots are left unquantified.

Contact Robert K. Squire (Ext. 7616) for further information on this article.

U.S. Strategic View

If one sets aside certain moralistic U.S. pronouncements on foreign policy and turns instead to the historical evidence and apparent operational reality behind U.S. deeds, it can be seen that this nation is as deeply committed to balance-of-power politics abroad as it is to the checks and balances principle in internal affairs at home.

The prevailing U.S. emphasis on checks and balances has deep historical roots and apparently derives – at least partly – from deep inner convictions about the nature of man and the perceived danger of excessive concentration of power. As Professor Richard Pipes, the noted Harvard historian, has observed: "The most striking illustration of America's faith in the balance-of-power principle was the decision to allow the Soviet Union to attain parity in nuclear weapons. It would be difficult to find, in the whole history of international relations, another instance of a country deliberately reducing its advantage over a rival for the sake of attaining an equilibrium."

The official U.S. view of that equilibrium – parity – was stated by President Nixon: "Those who scoff at balance of power diplomacy on the world scene should recognize that the only alternative to a balance of power is an imbalance of power, and history shows us that nothing so drastically escalates the danger of war as such an imbalance."

Thus the probability of war is perceived by the U.S. – or at least by many of this nation's leaders – to be minimum at parity. This is implicit

in our present SALT negotiations. But is this true? History provides too many examples of war breaking out between equal or essentially equal opponents. It could be suggested that violence between the very strong and the very weak is *less* likely than violence between equals -- in an unbalanced situation, the weak member won't start a fight, and the strong one need not. Further, even if the above view of parity were correct in some restricted sense, basing foreign policy on it might be dangerous if the other party in a specific contest holds a different view. Is it possible that this is the case for the U.S.S.R.?

Soviet Strategic View

What can we deduce about Soviet attitudes and beliefs? Our thoughts must be at least partly conditioned by the fact that today's Soviet government is but a modern embodiment of the autocratic, power-based rule that has been Russia's fate since Viking Prince Rurik established a kingdom in Kiev in the 8th century. While Europe was struggling upwards from feudalism and anti-intellectual religious orthodoxy into the liberal scientific-industrial age, Russia lay gripped by the Mongols. Ghengis Khan and his successors ruled there for a quarter millenium – a rule characterized by the maximum use of brutal power and arbitrary violence. No people could have survived the Mongols without gaining an appreciation for the effectiveness of violence and the dangers of being weak in the face of it.

Even after the Mongol yoke was thrown off in the 15th century, Russia continued to be the prey of predators. Never in its more-than-1000-year history has Russia had a single friendly neighbor; even little Lithuania once erupted as a military power and conquered her. As Stalin said on the eve of the first five-year plan, designed to prepare the U.S.S.R. for war with Germany: "The history of Russia is the history of defeats. She was beaten by the Mongol Khans, she was beaten by the Turkish Beys, she was beaten by the Swedish Feudal Barons, she was beaten by the Polish-Lithuanian Landowners, she was beaten by the Anglo-French Capitalists, she was beaten by the Japanese Barons. All beat her because of her . . . military backwardness."

But the benefits of military strength are also manifest in Russian history. Today, the U.S.S.R. is a colonial empire composed of many former nations and nationalities, among them the Tartars, Finno-Ugrians, Siberians, Ukrainian Cossacks, nomads of Central Asia, Crimeans, Ukrainians, Belorussians, Finns, Caucasians, and the Moslems of Turkestan. All have been brought under the rule of the Great Russians of Muscovy – sometimes by fighting, sometimes by coercion, but always by power. Today's Soviet government rules over this empire and claims even more – that it is the sole keeper of a faith by which all mankind shall be saved.

Given this history, is it possible for the Soviet leaders to view their long-range relationship with the U.S. in terms other than a continued power confrontation? It may be that the Soviets view parity as a threat to be overcome, not a situation to be embraced with equanimity.

Analysis

The dependence of war probability on the strategic force balance, the issue at hand, can be graphed as shown in Fig. 18. In this figure, the ordinate denotes the probability of war. The abscissa is strategic force balance running from the left, where "black" has forces but "red" none, through parity to the reverse situation at the right, where "red" has forces but "black" none. The condition at either extreme represents absolute military superiority.

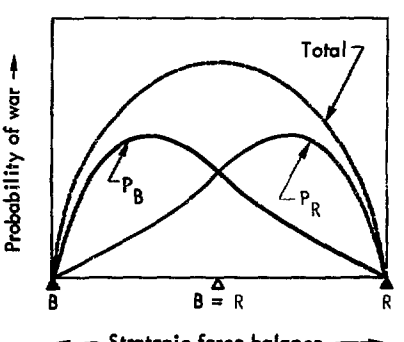

Fig. 18. In a bipolar confrontation, the total probability of war is the sum of probabilities that either side will initiate war. In this figure, the ordinate indicates the probability of war and the abscissa the strategic force balance: from absolute military supremacy of "black" (*left*) to absolute military supremacy of "red" (*right*). The individual probabilities of "black" and "red" initiating war are shown here as P_B and P_R, respectively; the total probability is the resulting upper curve. These curves are approximations. Because the intent is to communicate concepts rather than numerical probabilities, the coordinates are unquantified.

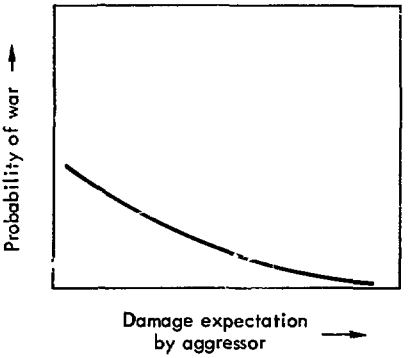

Fig. 19. Modern warfare has added the danger of catastrophic retaliatory damage to the other risks faced by an aggressor nation. The likely effect is to reduce the probability of war as the aggressor comes to believe he will suffer grievous damage whatever the outcome.

The overall probability of war consists of the component probabilities of either side initiating war. In Fig. 18, these components are plotted as P_B (the probability of black initiating war) and P_R (the probability of red initiating war). It seems plausible that, say for black, this probability rises from zero at the left, where war is unlikely because there are no red opposing forces and black can get its way without war, to a maximum well before parity*; the probability then falls to zero at the right where black has no forces and, hence, will not start a fight. There is a mirror *reflection around parity for red. The sum of these two* is the total probability of war, which is distinctly different from the individual probabilities for either of the two components. The total probability may be highest, not lowest, at or near parity.

If this analysis is consonant with history (and we believe it is), is it also applicable to today's world? To the usual risks faced by an aggressor nation, modern war has added the danger of catastrophic retaliatory damage. The likely effect of this knowledge on a potential aggressor is graphed in Fig. 19. It seems reasonable to expect the probability of war to decline as the aggressor comes to believe he will suffer grievous damage whatever the outcome. Presumably the probability of war goes to zero when this expectation reaches 100% – the so-called "Doomsday machine" deterrent.

Combining the concepts in Figs. 18 and 19 leads us to a three-dimensional plot (Fig. 20) in which a new axis – perceived probability of damage – is added. This chart shows the likelihood of war decreasing in relation to the aggressor's anticipation of retaliatory damage. We suggest this form as a structural framework for working problems of strategic arms procurement and control.

Because our main interest is the nuclear era, let us examine the past three decades using Fig. 20 as a map. Obviously the U.S. and U.S.S.R. have experienced different "nuclear histories," denoted by different arrows along the surface of the probability of war. The U.S. was essentially invulnerable to Soviet actions in 1945. Although the Soviets posed a threat to our friends in Europe and hence were not utterly powerless, war between the U.S. and U.S.S.R. would have resulted in relatively few American casualties. But this fact meant that the U.S. could successfully coerce the Soviet Union in many matters; thus, the probability that the U.S. would be driven to initiate war was very small.

The U.S. path from relative invulnerability in 1945 to a high expectation of damage and strategic parity in 1975 results from the Soviet acquisition of strategic nuclear weapons. The U.S. can now anticipate casualties of 50% or more in a strategic nuclear exchange; the inhibitions on U.S. initiative are real and obvious.

The Soviet Union, on the other hand, could only *have seen 1945 as an extraordinarily poor time* to attack the U.S. War would have produced heavy Soviet casualties and probably failure of her society. Their progression to 1975 has been accompanied by some increase in damage expectation because the U.S. has added to its strategic arsenal; however, the net change in position for the Soviets has been far less drastic than for us.

In 1960, Khrushchev called for a major Soviet armaments effort to "exceed the U.S. in all important measures of military power." In 1962, he was forced to acknowledge the penalty of Soviet strategic inferiority when the Cuban missile crisis erupted against a background of U.S. superiority in strategic arms. His successor in 197[illegible] can look with satisfaction to the fact that the U.S.S.R. has mastered strategic nuclear arms and matched or excelled the U.S. in such weaponry.

*In the prenuclear era, military doctrine called for a 3:1 superiority to ensure the success of an attack. In Fig. 18, this point occurs – for both black and red – well before parity.

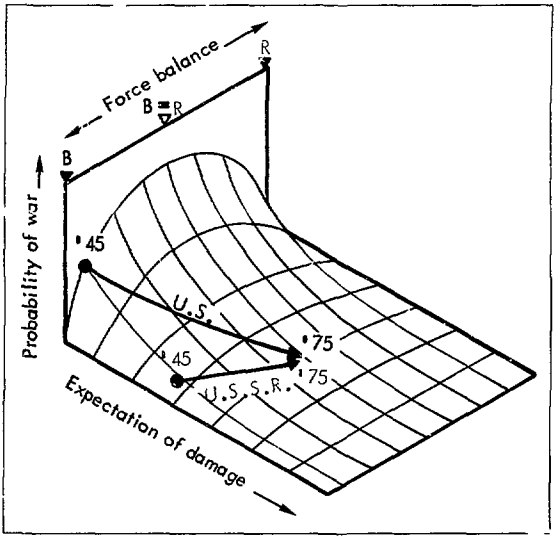

Fig. 20. The anticipation of damage by a potential aggressor adds a new dimension to the plot of war probability vs strategic-force balance. This chart traces the strategic nuclear histories of the United States and Soviet Union. Against a rising expectation by both nations of severe damage in a nuclear war, the Soviets have moved from a position of overwhelming inferiority to parity with the U.S. in strategic nuclear arms.

Future Possibilities

U.S. leadership tends to view our present strategic military relationship with the Soviet Union as one of mutual assured destruction (see Fig. 21). Advocates of this stance recommend parity at high armament levels and no protection of the respective societies from such weapons. The essence of this view is that both nations will eschew war if each sees that the other can inflict catastrophic damage to the attacker's society. Moreover, the U.S. predilection toward checks and balances provides a rationale for parity as the only reasonable solution to an otherwise unsolvable puzzle of the correct ratio of forces. As shown in Fig. 21, this solution suggests a low probability of war and the likelihood of severe damage to both nations if war occurs.

Infinite deterrence is another stance. Its advocates argue that the arms race is a good thing that cannot be overdone because it lessens the probability that deterrence will fail and war ensue. The essence is to increase the threat of damage to the aggressor's society, thereby increasing the penalty for initiating war.

Advocates of a return to U.S. strategic superiority can be found, especially among the more conservative political and military elements. The net desired effect is to reduce the probability that the Soviets will initiate war – damage potential remaining the same – by shifting the strategic force balance toward U.S. dominance.

Advocates of arms reduction focus on the danger that deterrence may fail. They speak of the humane reduction of death and destruction that would obtain from scaling down strategic arms in both number and effect. However, in the view offered here, this reduction in damage potential is accompanied by a necessary increase in the probability of war; that is, an increase in the probability that deterrence will in fact fail.

Which direction might the Soviet Union favor? Great care must be taken that our preconceptions don't prejudice our thoughts. At no time have the Soviets indicated they are halting production of strategic armaments or reducing their stockpiles. To a wealth of other observations about Soviet intentions can be added the following recent assessment to NATO by British Ambassador Malcolm Macintosh: "Any thought that parity or equivalence with the U.S. should turn the Soviet Union into a satisfied power, content to settle down with the U.S., Western Europe, and the rest of the world in an atmosphere of live and let live, is totally foreign to Soviet philosophies and outlooks. To the Russians, the U.S. is fundamentally a hostile

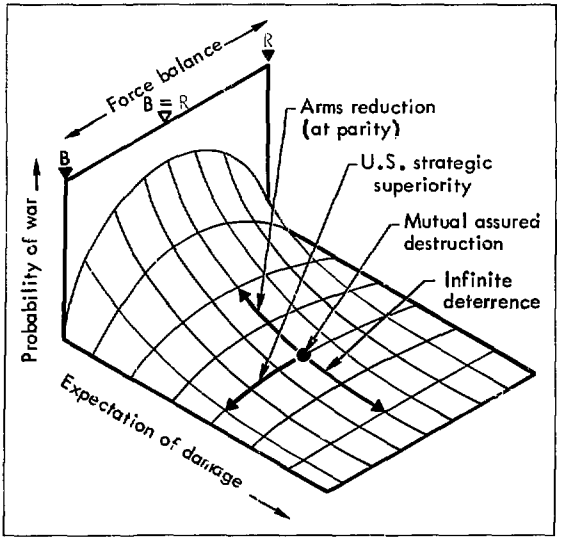

Fig. 21. Contradictory arguments are set forth within the U.S. as to which strategic nuclear path to follow. These positions are discussed in the text. The apparent effect of arms reduction at parity is to increase the probability of war by decreasing the ability of the U.S. and U.S.S.R. to inflict catastrophic damage on one another in case of nuclear war.

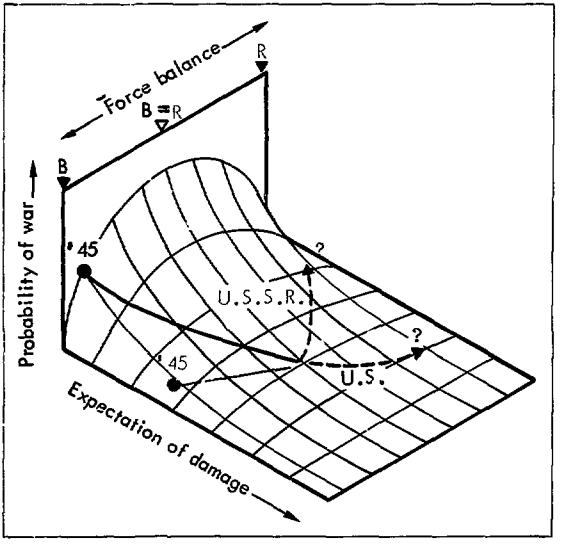

Fig. 22. If the U.S.S.R.'s goal is strategic nuclear superiority, the Soviets will push for weapons advantage, counter-force capability, ballistic missile defense of their cities, and effective civil defense. They will oppose U.S. efforts to achieve similar objectives. The net effect would be to put the Soviets into a position of maximum coercive leverage through a combination of their strategic superiority and U.S. vulnerability to nuclear attack.

power to be weakened and outwitted whenever possible." By way of corroboration, Foy Kohler, former U.S. ambassador to the Soviet Union, has said: "The Soviets have indicated that there's no place in their thinking for a static situation in their relationship with the U.S. They think of national power, including military power, in terms of a class struggle with the capitalists . . . fundamentally and irreconcilably opposed until the defeat of capitalism."

One interpretation of the Soviet climb from *inferiority to strategic military parity with the U.S.* is that parity is a necessary way station en route to strategic superiority. From this position they may hope, in an historic turnabout, to strive for global supremacy. This view is charted in Fig. 22 – the Soviet "path" moving toward strategic superiority and minimum threat of damage, and their preferred path for the U.S. (the one they would hope to force the U.S. to follow) moving toward strategic inferiority and heavy threat of damage. If this interpretation is correct, we can expect the Soviets to strive – over the years – for strategic superiority, counterforce capability, ballistic missile defense of Soviet cities, and a large civil defense program. Correspondingly, we can expect them to oppose U.S. efforts to maintain parity, oppose a significant U.S. counterforce capability, oppose a U.S. ballistic missile defense of cities or strategic forces, and oppose a U.S. civil defense program.

Over the long range, the results of negotiations, military R&D, Soviet deployments, etc., will confirm or deny this interpretation. It is not the purpose of this paper to analyze these options, but the danger is clear: if the Soviets are in fact moving toward strategic superiority and if the analytical approach of this paper is correct, it behooves us to respond such that they do not achieve their ends. One would hope to do so without increasing the damage potential or the probability of nuclear war.

In conclusion, it appears possible – perhaps even probable – that the U.S. and U.S.S.R. are operating on entirely different perceptions of the meaning and future of strategic force relationships. It seems unlikely that the Soviets will embrace parity as a stable or desirable relationship with the U.S. They may be striving for strategic superiority and damage-limiting capabilities; if so, the U.S. response will have to search beyond parity and mutual assured destruction for more enduring strategic policies.

Key Words: strategic force balance; arms control; nuclear warfare – damage expectation; military policy – U.S.; military policy – Soviet.

Notes and References

1. G. Sommargren, *J. Opt. Soc. Am.* **65**, 960 (1975). Note that in this analysis, θ is changing at a constant rate to produce a frequency shift.
2. D. Lager and R. Lytle, *Computer Algorithms Useful for Determining a Subsurface Electrical Profile Via High-Frequency Probing*, Lawrence Livermore Laboratory Rept. UCRL-51748 (1975).
3. R. Lytle, D. Lager, E. Laine, and J. Salisbury, *Monitoring Fluid Flow by Using High-Frequency Electromagnetic Probing*, Lawrence Livermore Laboratory Rept. UCRL-51979 (in preparation).
4. E. Laine, J. Salisbury, and R. Lytle, *Near-Field Corrections in Conducting Media Programmed for a Pocket Calculator*, Lawrence Livermore Laboratory Rept. UCRL-77668 (in preparation).
5. E. Laine and R. Lytle, *A Computer Program for Four-Probe Resistivity Measurements in a Horizontally Layered Earth*, Lawrence Livermore Laboratory Rept. UCRL-51997 (in preparation).